Materials Research. 2015; 18(1): 212-221
DOI: http://dx.doi.org/10.1590/1516-1439.332914

Microstructure and Properties of Nickel-based C276 Alloy Coatings by PTA on AISI 316L and API 5L X70 Steel Substrates

Luciano da Silva Ferreira[a], Karin Graf[b], Adriano Scheid[b]*

[a]Graduate in Mechanical Engineering – PGMec, Federal University of Paraná – UFPR, Curitiba, PR, Brazil
[b]Department of Mechanical Engineering, Federal University of Paraná – UFPR, Curitiba, PR, Brazil

Received: September 24, 2014; Revised: January 27, 2015

This work assessed Ni-based C276 alloy coatings by PTA with different degree of interaction with AISI 316L and API 5L X70 steel substrates. Track geometry, dilution and microstructure of coatings were evaluated by optical, scanning electron microscopy and X-ray diffraction. Properties were evaluated by hardness and wear tests. Microstructure exhibited austenite Ni-FCC dendrites and interdendrictic regions containing carbides. Dilution from 4,9 to 25,4% for coatings on API 5L X70 leaded to hardness ranging from 283 to 243 $HV_{0,5}$. Otherwise, dilution between 22,3 and 41,5% for coatings on AISI 316L induced hardness from 267 to 225 $HV_{0,5}$. Higher interaction with the substrate leaded to 19,8% increase of mass loss rate on API 5L X70 coatings. The slight difference for coatings properties deposited on different substrates indicated that the degree of interaction was the most significant factor.

Keywords: *microstructure, hardness, Ni-based coatings, C276 alloy, plasma transferred arc, substrate interaction*

1. Introduction

Coatings have been applied to protect components surface in different applications[1]. Nickel-based alloys are used to extend campaign of engineering components in many industrial areas including chemical processing, nuclear power plants, marine engineering and oil and gas industry, mainly involving corrosion and/or heat resistance[2-5]. Gas and oil facilities usually submit components to operate in aggressive environments which may involve corrosion, stress corrosion cracking and corrosion-fatigue[2,3,6-8].

The Nickel-Chromium-Molybdenum C276 alloy has high Molybdenum content on chemical composition to improve chloride attack resistance and, therefore, resulting higher pitting resistance. Together with Molybdenum, Tungsten is a solid solution strengthener providing high strength without heat treatment. Both, as strong carbide formers, also contribute to enhance mechanical properties throughout formation of hard phases[3].

Besides the effect of solid solution and second phase (carbide) on strengthening, Chromium contents higher than 15% improve oxidation and carburization resistance because of the formation of a protective oxide layer on the surface. The Nickel base of the alloy allows the retention of this formed superficial protective layer, especially on cyclic exposures at high temperature[3,6-10].

Rolling cladding is largely utilized to produce coated steel sheet components attending different corrosion requirements. Additionally, welding processes like plasma transferred Arc (PTA) have been studied as an alternative due to the high quality of deposits[3,11-13]. When a welding process is involved, the effect of substrate and the degree of interaction due to processing parameters (measured by dilution) has to be taken into account[14,15]. All these factors alter the chemical composition of coatings and, consequently, the microstructure, impacting on coatings properties[7-10].

This work evaluated the effect of substrate on characteristics of Nickel-based coatings by plasma transferred arc thru processing current intensity variation in order to achieve different interaction degrees (dilution) with the substrate. For this study, C276 alloy coatings were deposited on AISI 316L and API 5L X70 steels utilizing three deposition current intensities: 120, 150 and 180A. Coatings were characterized by track geometry, microstructure and phases formed. The impact of coatings microstructure on properties was assessed by hardness and abrasive sliding wear tests.

2. Experimental Procedures

Nickel-based alloy was deposited by PTA with a starweld PTA 300M equipment using the commercial atomized alloy of Stellite kown as Hastelloy C276, with grain size ranging from 90 to 150μm on AISI 316L stainless steel 12,5mm thick and API 5L X70 steel 10,0mm thick plates. The chemical composition of the materials is shown in Table 1.

*e-mail: scheid@ufpr.br

Table 1. Chemical composition of the materials used (wt.%).

Ni-Based Alloy									
Element	**Ni**	**Cr**	**W**	**Mo**	**C**	**Fe**	**V**	**Si**	**Mn**
NiCrMo C276 alloy	Bal.	15.4	4.5	15.9	0.10	3.1	0.6	0.6	1.1
Steel Substrates									
Substrate 1	**Fe**	**C**	**Mn**	**Si**	**P**	**S**	**Cr**	**Ni**	**Mo**
AISI 316L	Bal.	0.02	1.35	0.43	0.03	0.008	16.78	10.1	2.1
Substrate 2	**Fe**	**C**	**Mn**	**Si**	**P**	**S**	**Cr**	**Ti**	**Nb**
API 5L X70	Bal.	0.17	1.40	0.21	0.02	0.003	0.005	0.015	0.041

Single tracks with 100 mm length were processed according to parameters presented in Table 2. Characterization was carried out in the middle length of the track, discarding 20 mm of the deposits extremities. Track geometry was evaluated by optical microscopy concerning the reinforcement thickness (t), width (W) and wettability angle (Θ), Figure 1. The degree of interaction with the substrate was measured by dilution. It was expressed as the ratio between melted substrate area and total melted area (areas method) on the cross section of coatings.

For each deposited condition (120, 150 and 180A), cross section samples were cut out and metallographic prepared by grinding, polishing and etching. Optical microscopy for microstructure evaluation was done in the as-deposited coatings for phase identification and quantification. The volume fraction of hard phase was measured as an average of 5 samples, under 500 X magnification, by Olympus Soft Imaging Solutions® software. X-ray diffraction (XRD) analysis on the grinded top surface of the coatings was carried out with K_{α}Cu radiation from 20 to 120º with 1 s time of exposure channel. Vickers hardness of the coatings was measured on the transverse cross-section under 4,9 N load as the average of 10 measurements.

Coatings wear behavior was evaluated in homemade equipment. The sliding test considered silicon carbide paper (#600) assembled on a 63 HRC hardness metal disc as the counterpart, run with 4,9 N axial load and a 1,5 m/s tangential speed. Pins with a transverse cross section of 4 x 4 mm were machined from the deposited coatings. Pins mass loss was determined by weighting them before beginning every test and after each 125 m sliding distance, up to 375 m, at room temperature. The main purpose of wear tests was to evaluate the effect of substrate and degree of interaction (dilution) on coatings performance.

Table 2. Plasma Transferred Arc processing parameters.

Parameters	
Shielding gas (l/min)	2
Protection gas (l/min)	15
Powder feeding gas (l/min)	2
Main arc current (A)	120, 150, 180
Powder feed rate	Constant in volume
Travel speed (mm/min)	100
Distance torch / substrate (mm)	10
Electrode diameter (mm)	3.125

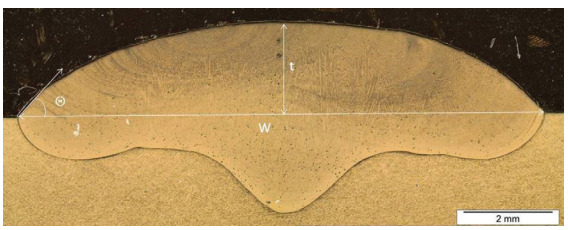

Figure 1. Geometry of welding overlays: thickness (t), width (w) and wettability angle (Θ).

3. Results and Discussion

3.1. Coating soundness

Visual inspection of deposited coatings on both substrates revealed smooth surfaces with no macroscopic processing defects like porosities, cracks, lack of fusion or undercut, Figure 1. This macroscopic evaluation is coherent with literature predictions concerning the integrity of NiCrMo alloy coatings[15]. Otherwise, knowledge about the effect of substrate and its processing interaction (measured by dilution) on microstructure and properties of C276 alloy coatings is still limited.

Nickel-based alloy presented differences on geometry of single track coatings as a consequence of deposition current variation and substrate. As expected, the lowest wettability was measured processing NiCrMo C276 alloy with 120 A, confirmed by the highest wettability angle (Θ), reinforcement thickness (t) and shallowest width compared to coatings processed with higher current (150 and 180A), Table 3. Following predictions, the higher thermal conductivity of carbon API 5L X70 steel leaded to a decrease on coatings wettability that was more significant for higher current intensities[15].

3.2. Effect of substrate and dilution on microstructure

As expected, interaction with the substrate (dilution) increased with the deposition current [15] and measured values ranged from 4,9 to 41,5%, Table 3. The superior interaction observed for coatings on AISI 316L was a consequence of

Table 3. Geometry and dilution of welding track for NiCrMo coatings.

Substrate	Evaluation	Deposition Current (A)		
		120	**150**	**180**
AISI 316L	Dilution	22.3	35.9	41.5
	Thickness (t)	2.9	2.4	2.1
	Width (W)	9.1	11.9	11.9
	Wettability Angle (Θ)	63.0	46.6	43.3
API 5L X70	Dilution	4.9	13.2	25.4
	Thickness (t)	2.8	3.1	2.8
	Width (W)	8.4	9.7	11.0
	Wettability Angle (Θ)	64.9	51.0	48.0

the lower thermal conductivity of the austenitic stainless steel. Once the interaction with the substrate (dilution) is strongly dependent on deposition current and substrate, it will dictate solid solution, second phase and their distribution on coatings[14,15].

As Iron atoms (solute) can easily substitute Nickel atoms (solvent) in the crystal structure, substitutional solid solution, the higher interaction with the substrate leaded to coatings with larger areas of Ni-FCC dendrites, reducing the proportional amount of alloying elements as Molybdenum, Tungsten and Chromium, Table 4[6,13-15]. X-ray diffraction analysis revealed the presence of a [Ni, Fe]-FCC phase and different carbides on coatings, Figure 2 and Figure 3.

Microstructure of the coatings on AISI 316 L showed interdendrictic white MC (M: Molybdenum, Tungsten) and gray $M_{23}C_6$ (M: Chromium) primary blocky carbides, as a consequence of the higher dilution and lower cooling rate during solidification, Figure 4, Figure 5 and Figure 6. $M_{23}C_6$ carbides are expected when high amounts of Chromium are available during solidification. Its chemistry may range from simple Nickel-Chromium to $Cr_{23}(Mo,W)_2C_6$ as Molybdenum and Tungsten are available[16]. As dilution increases, more interaction with the substrate occurs and higher amount of Chromium become available to form this type of carbide. This interaction is also facilitated by the lower thermal conductivity of AISI 316 L stainless steel, which induces slower cooling rate on solidification.

Furthermore, deposits on API 5L X70 steel formed predominantly M_6C carbide (M: Iron-Tungsten (Fe_3W_3C)) with eutectic lamellar morphology, Figure 7, Figure 8 and Figure 9. Also known as eta (η) carbide, the M_6C carbide is usually formed when refractory elements like Molybdenum and Tungsten are available and the matrix is rich in elements like Nickel, Iron and Chromium[16]. Carbon content may alter the stoihciometry form, which may vary from Ni_3Mo_3C to Ni_2W_4C[16]. Lower amount of blocky MC (M: Molybdenum, Tungsten) and $M_{23}C_6$ (M: Chromium) carbides were also found due to the lower amounts of Chromium. Lamellar M_6C carbides on API 5L X70 steel substrate resulted from the higher carbon contents available on the melted pool diffusing from the substrate and the higher cooling rate during solidification, as a result of the highest thermal conductivity of this steel substrate[3].

Once the interaction with the substrate (dilution) was influenced by deposition current and thermal conductivity

Table 4. Chemical distribution by EDS on microstructure of Ni-Based coatings.

I (A)	Coatings on AISI 316L				
	Ni	**Fe D**	**Cr D**	**W D**	**Mo D**
120	Bal.	17.00	15.91	0.73	7.70
150	Bal.	31.93	16.11	0.67	6.61
180	Bal.	35.81	16.20	0.46	6.19
I (A)	**Coatings on API 5L X70**				
	Ni	**Fe D**	**Cr D**	**W D**	**Mo D**
120	Bal.	8.47	15.21	1.00	10.36
150	Bal.	21.63	13.50	0.71	8.53
180	Bal.	24.56	10.37	0.57	6.77

M D: where M is the metal and D indicates punctual analysis by EDS on Dendrites.

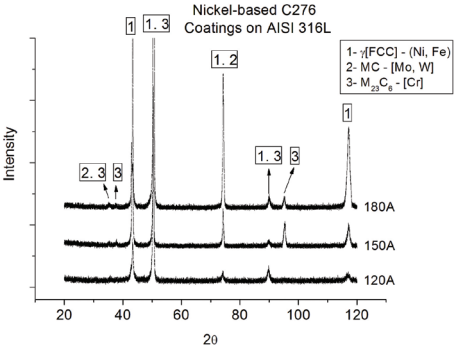

Figure 2. X-ray diffraction analysis on NiCrMo coatings deposited with 120, 150 and 180 A on AISI 316L.

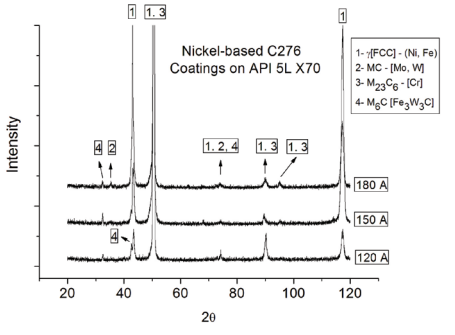

Figure 3. X-ray diffraction analysis on NiCrMo coatings deposited with 120, 150 and 180 A on API 5L X70.

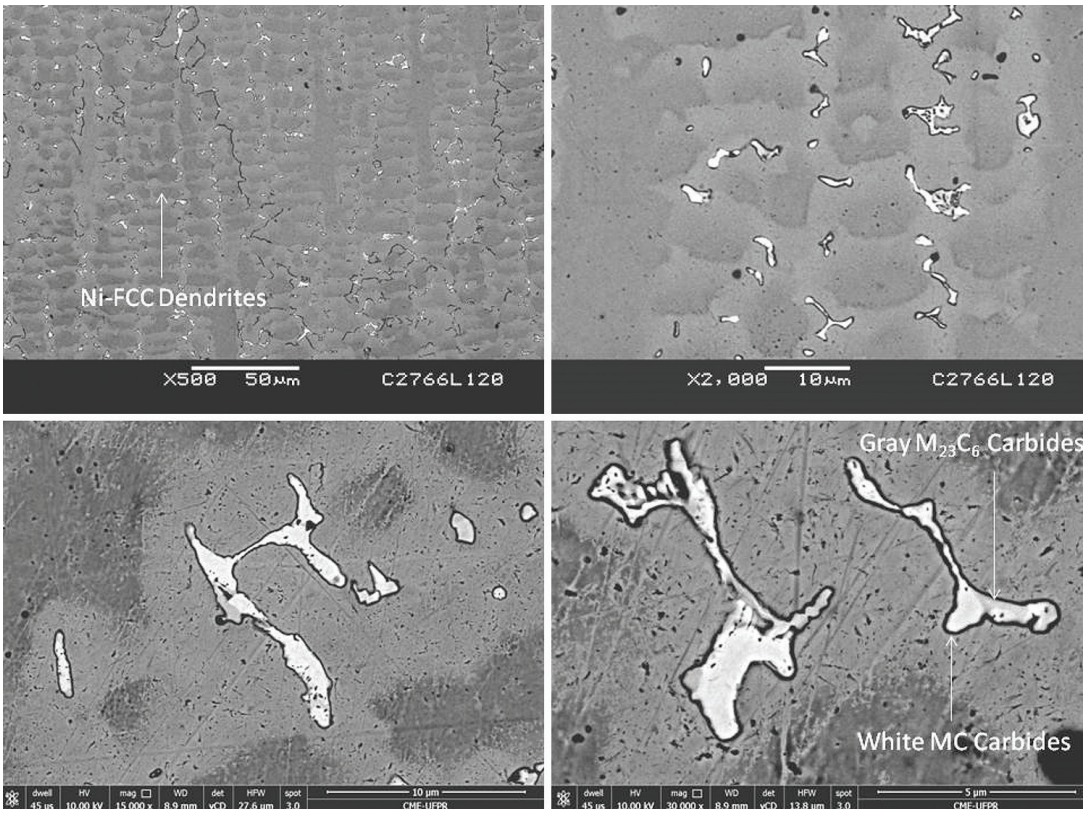

Figure 4. Microstructure of NiCrMo PTA coatings on AISI 316L (120 A).

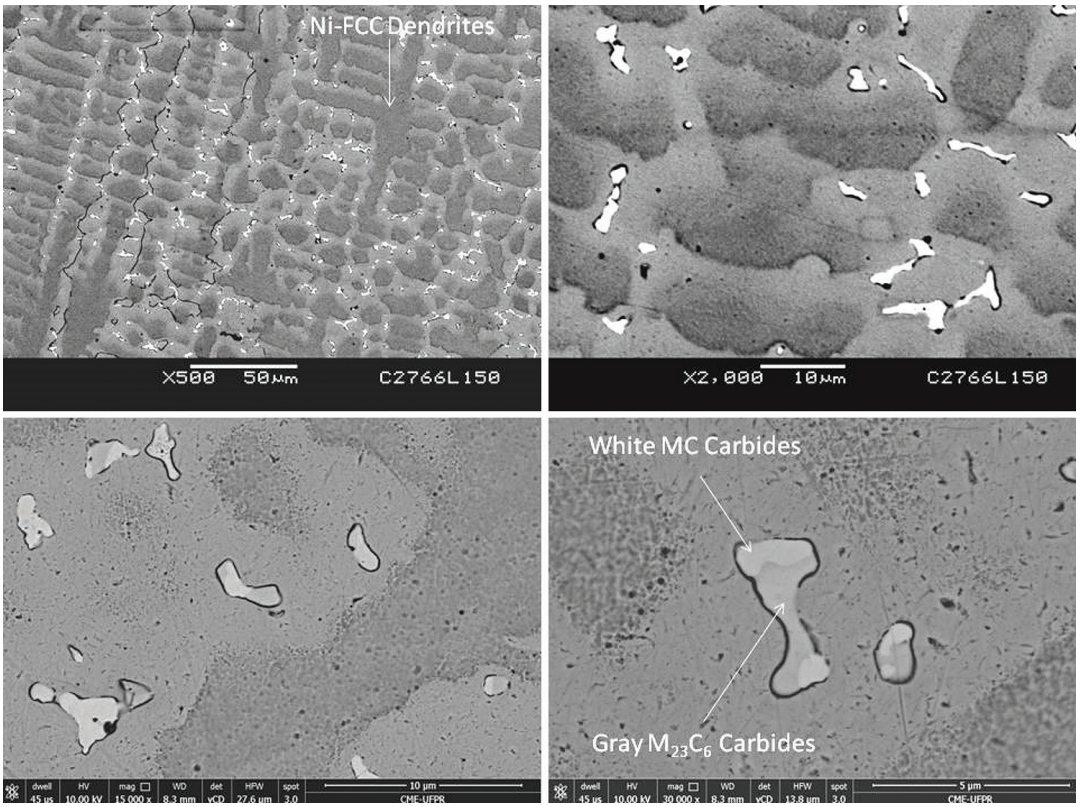

Figure 5. Microstructure of NiCrMo PTA coatings on AISI 316L (150 A).

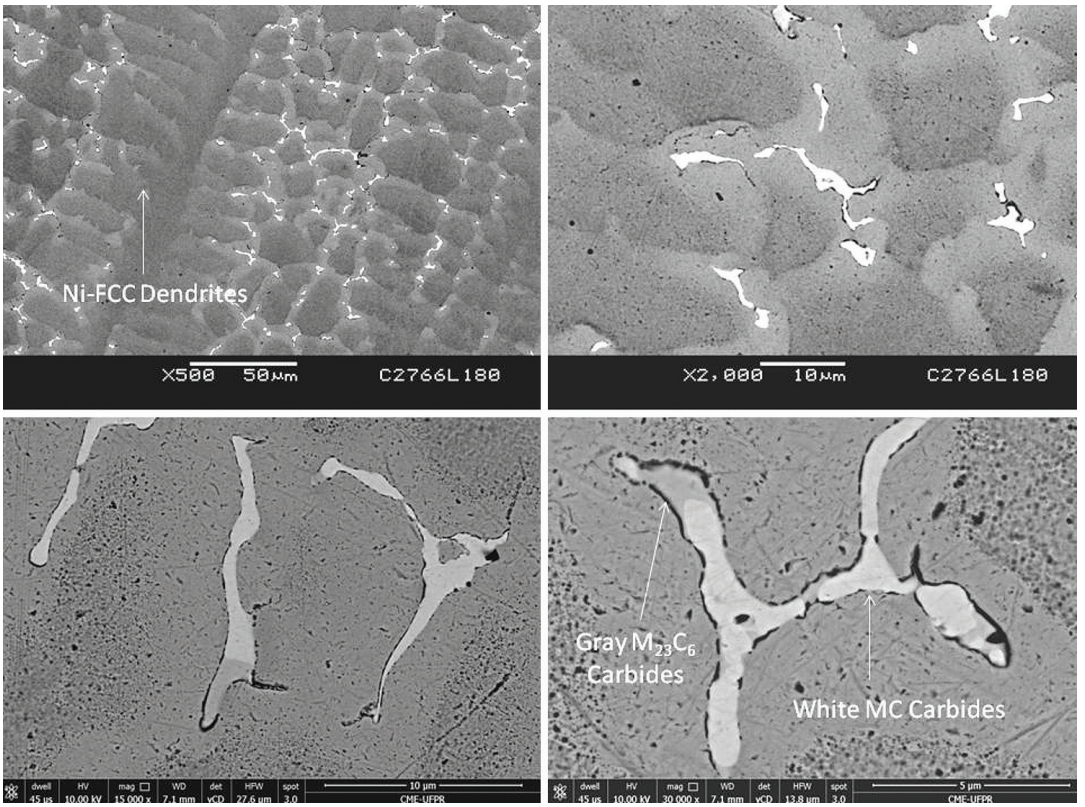

Figure 6. Microstructure of NiCrMo PTA coatings on AISI 316L (180 A).

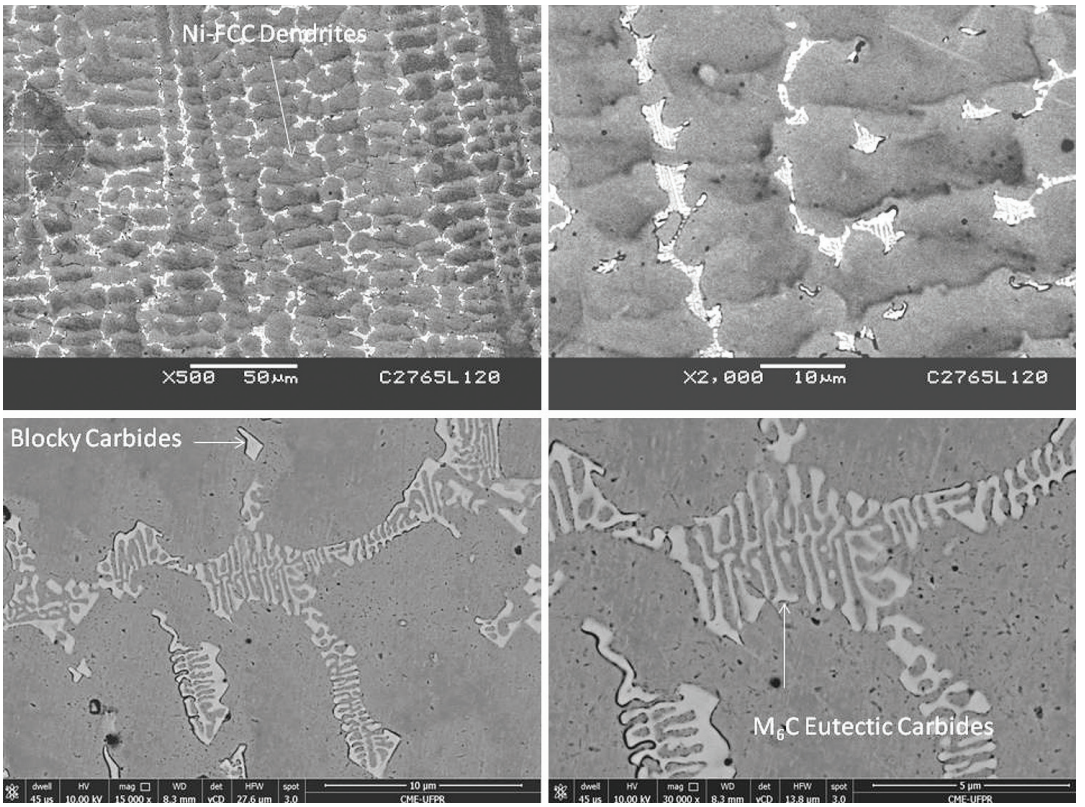

Figure 7. Microstructure of NiCrMo PTA coatings on API 5L X70 (120 A).

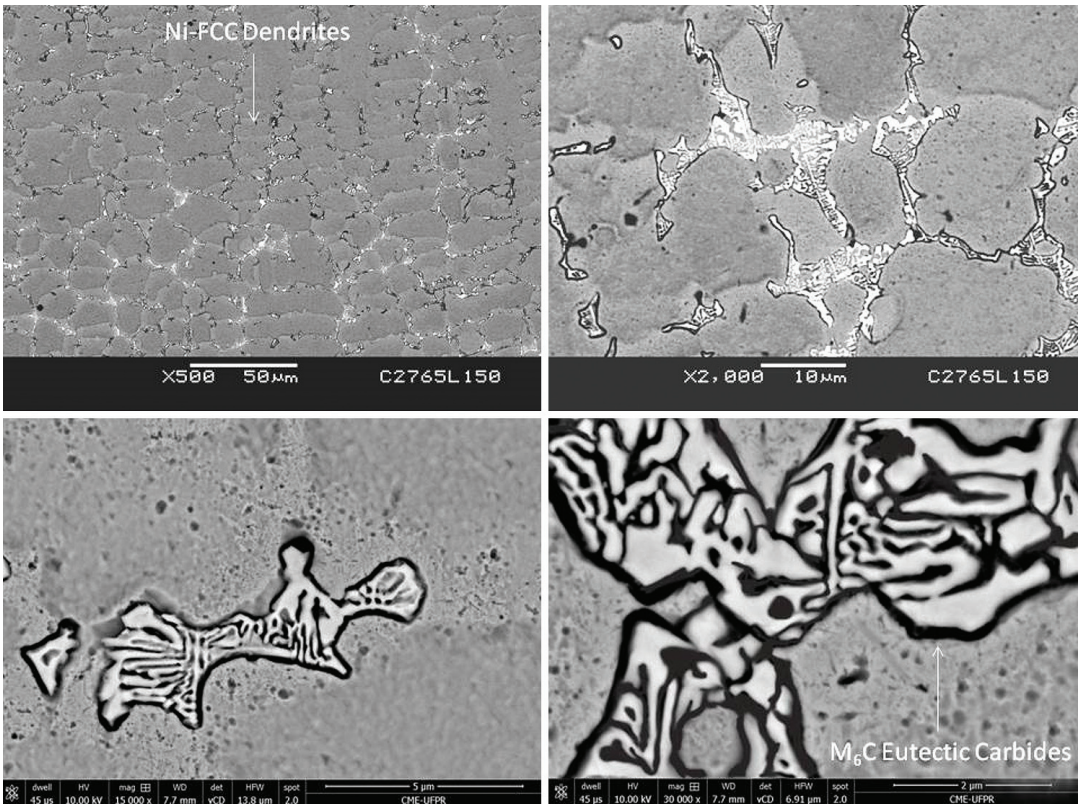

Figure 8. Microstructure of NiCrMo PTA coatings on API 5L X70 (150 A).

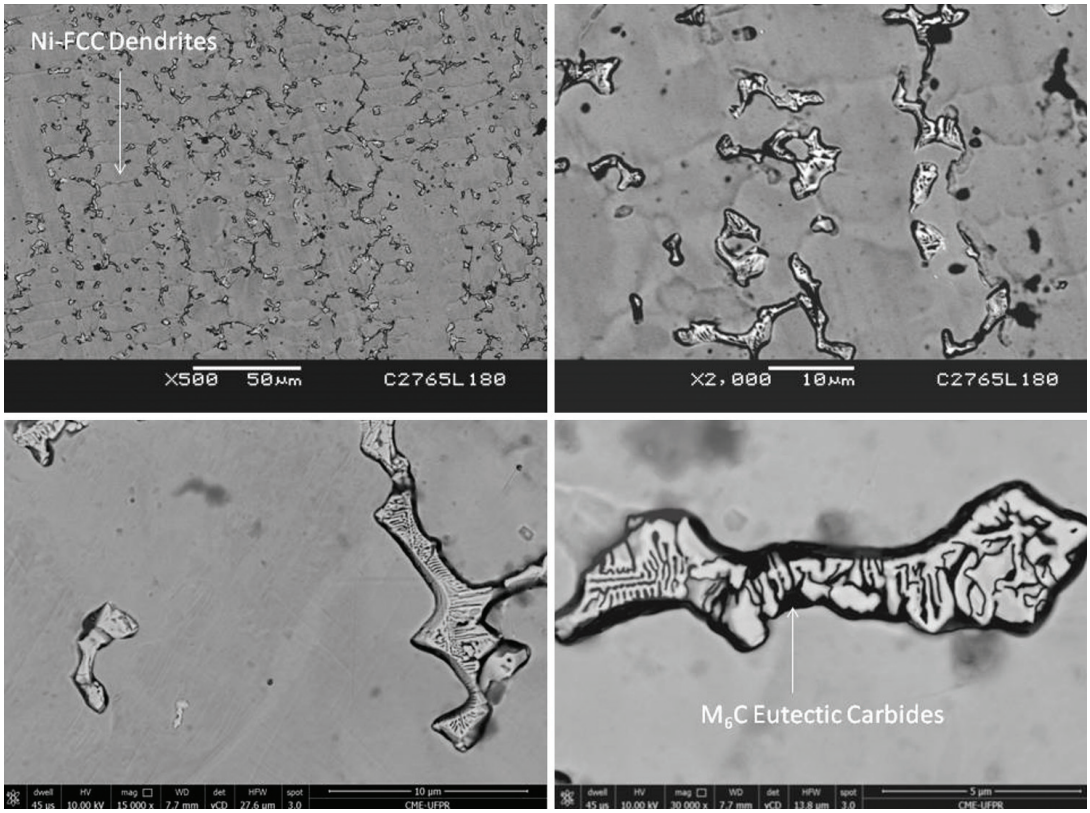

Figure 9. Microstructure of NiCrMo PTA coatings on API 5L X70 (180 A).

of the steel substrate, different Iron content (wt %) on coatings changed the alloying and the volume fraction of carbide formed, Figure 10. So, the higher deposition current the larger decrease of carbides fraction on coatings. Furthermore, the lower Carbon content of the AISI 316L (0,02 wt%) substrate dictated the reduced volume fraction of carbides on coatings when compared to API 5L X70 steel[6,7].

Dendrite arm spacing of Ni-FCC was altered by the deposition current and thermal conductivity of steel substrate. Both influenced the temperature of the substrate and so, the cooling rate of the coatings, Figure 11, and therefore, the distribution of interdendrictic carbides[15].

3.3. Effect of microstructure on hardness and wear performance

Once coatings microstructure was influenced by steel substrate and its interaction degree, hardness should be modified in same way. The higher dilution and the lower thermal conductivity of steel substrate, the lower hardness observed, Figure 12 and Figure 13. Interaction with the substrate depended on deposition current and thermal conductivity of substrate. So, chemical composition and cooling rate on solidification were altered. As a consequence, three different factors dictated hardness: solid solution alloying, carbide fraction and dendrite arm spacing.

Coatings deposited on the lower thermal conductivity AISI 316 L steel substrate presented higher dilution and reducing solid solution alloying. The low Carbon content of substrate leaded to the lower fraction of formed carbides. Finally, slower solidification cooling rate resulted from the lower thermal conductivity of substrate, inducing larger dendrite arm spacing. As expected, the lower hardness was observed for coatings on this substrate[15].

Ni-based alloy presented a decrease on mean hardness from 283 to 243 and from 267 to 225 $HV_{0,5}$ for deposits on API 5L X70 and AISI 316L respectively, as a result of higher dilution levels and coarser microstructures. Coatings on API 5L X70 steel substrate exhibited hardness up to 8% superior than on AISI316 L stainless steel while the difference from deposition with 120 and 180 A reached 15% hardness reduction for both substrates. It indicates that interaction with the substrate (dilution) is the most significant factor influencing hardness[3,10,15].

Considering Carbon content of C276 alloy powder (0,10 wt %) and the Carbon content of substrates (0,02 wt % and 0,17 wt %), low carbide fraction on coatings were measured, varying from 1,81 to 3,59%. The higher dilution and lower amounts of Carbon content on AISI 316 L substrate, induced carbides fraction decreased from 2,17 to 1,81% for 120 and 180 A, respectively. For the same range of deposition current, coatings on API 5L X70 presented higher variation of carbide fraction, between 3,59 and 2,39%. Despite the higher volume and different kind of carbides observed when comparing the coatings on different substrates, a lower hardness difference was observed.

Different degree of refinement was observed processing the coatings on substrates with different thermal conductivity. Dendrite arm spacing varied from 7,9 to 13,0 µm for coatings on AISI 316 L and from 6,2 to 9,4 µm for coatings on

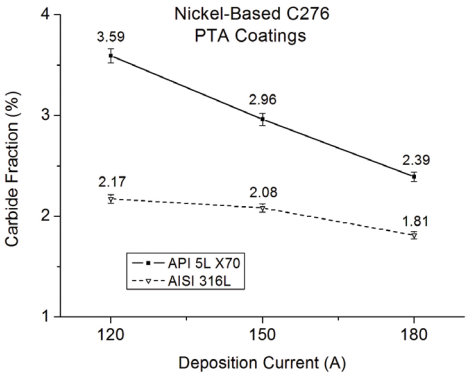

Figure 10. Interdendrictic carbide fraction on coatings.

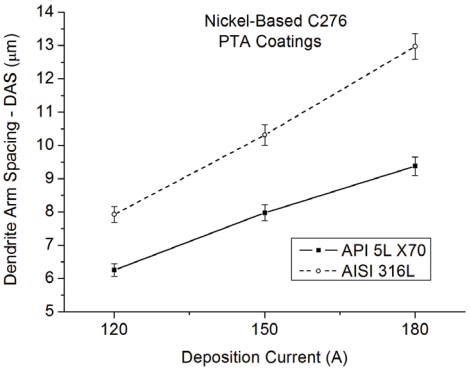

Figure 11. Dendrite Arm Spacing on transverse section of coatings.

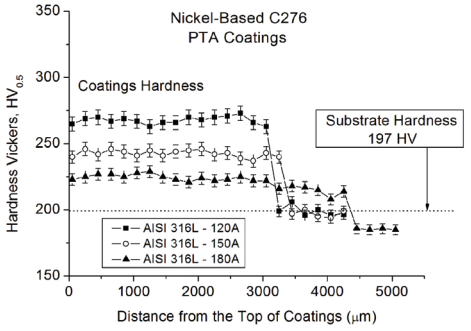

Figure 12. Vickers Hardness cross-section profiles for coatings on AISI 316L.

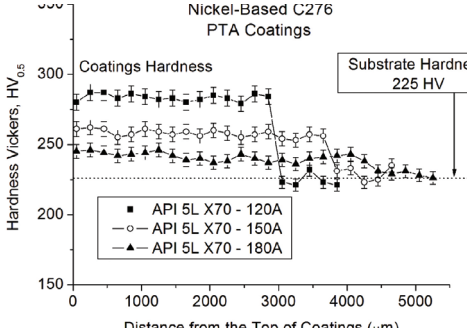

Figure 13. Vickers Hardness cross-section profiles for coatings on API 5L X70.

API 5L X70. It was influenced the extent of Ni-FCC carbide free areas and the distribution of interdendrictic carbides.

Moreover, the reduction on solid solution alloying was also verified as a consequence of interaction with the substrate, reducing the amount of Chromium, Molybdenum and Tungsten for coatings on API 5L X70 and Molybdenum and Tungsten for deposits on AISI 316 L steel, Table 4. Therefore, hardness was also influenced by the amount of solid solution alloying on Ni-FCC dendrites, as previously reported by literature[9-11,15].

Aiming to identify the influence of PTA deposition current and substrate on coatings response to abrasive sliding wear, coatings were tested in the as-deposited condition with a constant set of testing parameters. The microstructure and hardness changes obtained as a consequence of processing with higher current induced increasing mass loss rate, Figure 14 (a) to (d). Under tested conditions, a linear correlation between sliding distance and mass loss was observed and a near constant wear rate were measured with increasing sliding distance, in agreement to literature reports[12]. The results abided by Holm-Archard equation[17], which establishes that the volume wear is inversely proportional to the hardness.

The chemical composition of the Ni-based C276 alloy developed on coatings influenced the mass loss rate, being the processed with 120 A deposition current (lower dilution) the one that showed the lower wear rate of 0,0455 mg/m (on API 5L X70) and 0,0474 mg/m (on AISI 316 L). As the dilution increased for coatings with 180 A, the mass loss coefficient reached 0,0548 and 0,0545 mg/m, respectively. Superior behavior of coatings deposited with 120 A current can be associated to higher hardness measured. It was related to the larger volume fraction of carbides, higher solid solution alloying and lower dendrite arm spacing[15].

The larger interaction with the substrate obtained when increasing the current from 120 to 180 A increased the mass loss rate about 15,6% for coatings on AISI 316 L and 19,8% on API 5L X70 steel. Following the trend for the mean hardness, lower differences on wear mass loss rate ($\leq 4\%$) was observed comparing coatings on different steel substrate, Figure 15.

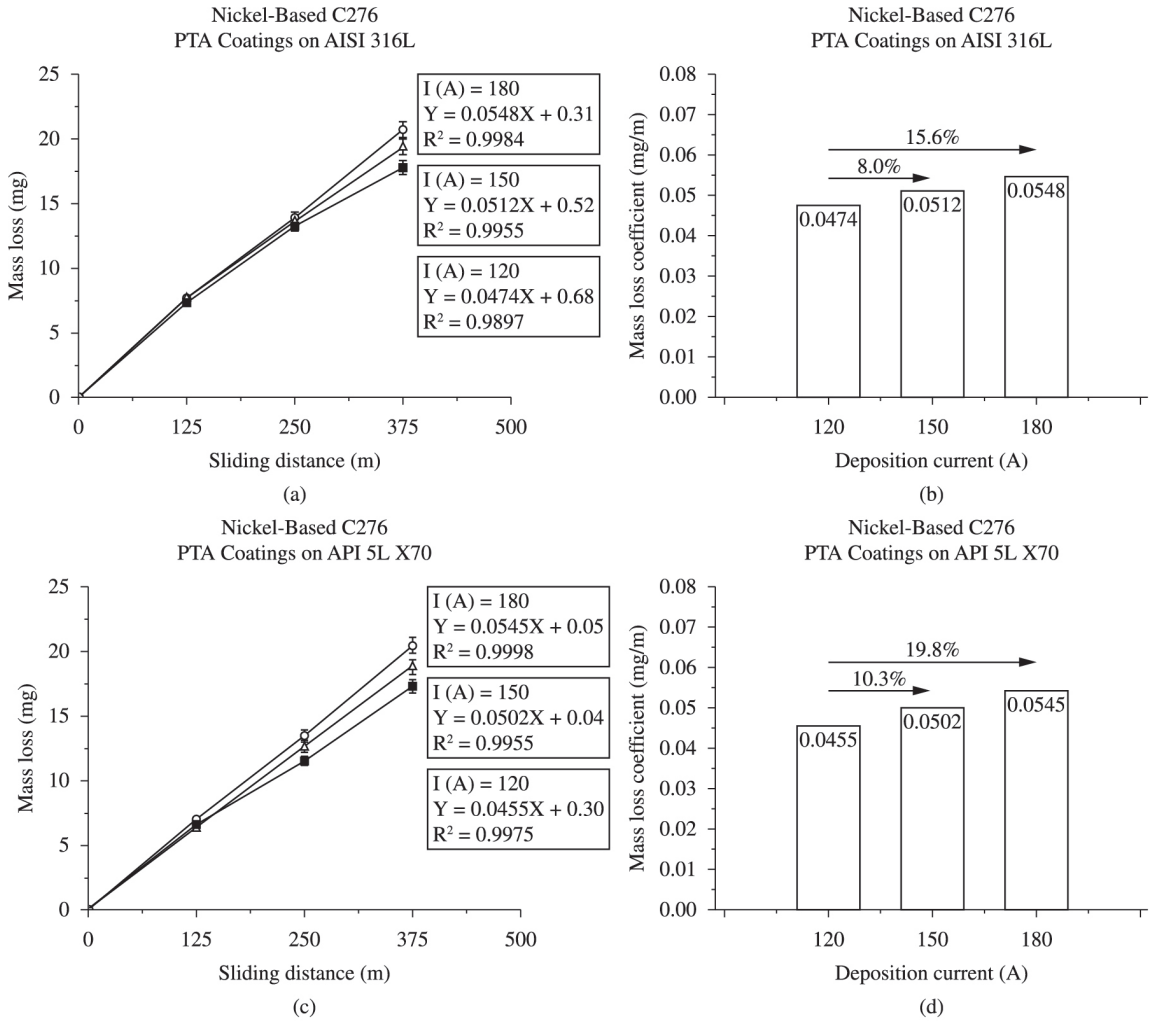

Figure 14. Wear curves and mass loss coefficient for coatings: (a) and (b) on AISI 316L and (c) and (d) on API 5L X70 substrate.

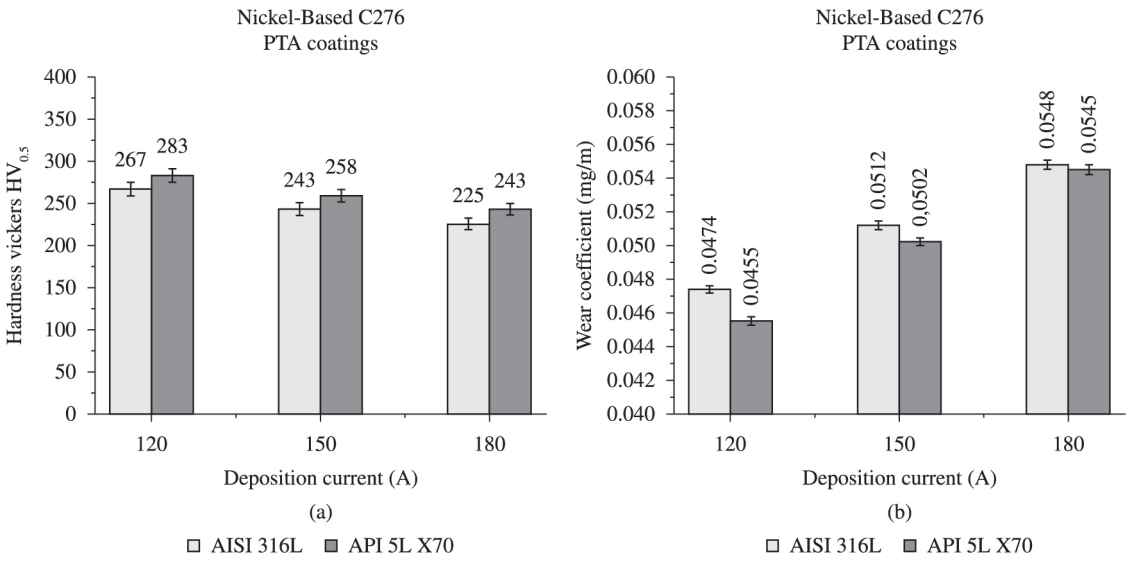

Figure 15. Correlation between coatings on AISI 316L and API 5L X70 for different deposition current.

4. Final Remarks

This study analyzed Nickel-based C276 coatings by PTA processed on API 5L X70 and AISI 316 L steel substrates with different degree of interaction on track geometry, microstructure, hardness and wear performance. The main conclusions are as follows:

- The Nickel-based alloy processed by PTA on API 5L X70 and AISI 316 L stainless steel plates showed correlation between substrate and track geometry. Coating integrity was influenced neither by the substrate nor by the interaction degree.
- Coatings Iron content was dictated by interaction degree with the substrate, which increased with the deposition current. The higher Iron content induced hardness decrease, mainly because of carbide fraction reduction and also due to the higher Iron content in dendritic solid solution.
- The thermal conductivity of the steel substrate influenced the dilution and dendrite arm spacing. Coatings on stainless steel presented coarsened microstructure, reduced carbide fraction and reduced solid solution alloying.
- The kind of interdendrictic carbides formed was dictated by the substrate which altered the solidification cooling rate and composition of coatings. Chromium $M_{23}C_6$ and Molibdenum-Tungsten MC blocky carbides were found on coatings for slow cooling rate and low Carbon AISI 316 L steel. Higher cooling rate on solidification and carbon content of API 5L X70 steel induced the predominant Iron-Tungsten (M_6C) lamellar carbide.
- Despite the influence of the substrate on the nature of interdendrictic carbides, interaction degree was the most important factor influencing the hardness and wear properties of C276 alloy coatings.

Acknowledgements

Authors would like to thank Fundação Araucária for financial support, agreement 425/2012.

5. References

1. Gonçalves RH and Dutra JC. PTA-P process - a literature review as basis for innovations. Part 2 of 2: powder thermal and kinematic behavior, process parameters and consumables. *Soldagem e Inspeção*. 2012; 17:173-183.
2. Smith L. Control of corrosion in oil and gas production tubing. In: Proceedings of the Materials Congress 98; 1998; Cirencester, Uk. Cirencester, UK; 1998.
3. Mankins WL and Lamb S. Nickel and nickel alloys. In: ASM International. *Properties and selection: nonferrous alloys and special-purposed materials*. Ohio: Materials Park; 1990. p. 1363-1403.
4. Liyanage T, Fisher G and Gerlich AP. Microstructures and abrasive wear performance of PTAW deposited Ni–WC overlays using different Ni-alloy chemistries. *Wear*. 2012; 274-275:345-354. http://dx.doi.org/10.1016/j.wear.2011.10.001.
5. Gurumoorthy K, Kamaraj M, Rao KP and Venugopal S. Microstructure and wear characteristics of nickel based hardfacing alloys deposited by plasma transferred arc welding. *Materials Science and Technology*. 2006; 22(8):975-980. http://dx.doi.org/10.1179/174328406X100734.
6. Fernandes F, Lopes B, Cavaleiro A, Ramalho A and Loureiro A. Effect of arc current on microstructure and wear characteristics of a Ni-based coating deposited by PTA on gray cast iron. *Surface and Coatings Technology*. 2011; 205(16):4094-4106. http://dx.doi.org/10.1016/j.surfcoat.2011.03.008.
7. Fernandes F, Cavaleiro A and Loureiro A. Oxidation behavior of Ni-based coatings deposited by PTA on gray cast iron. *Surface and Coatings Technology*. 2012; 207:196-203. http://dx.doi.org/10.1016/j.surfcoat.2012.06.070.
8. Gatto A, Bassoli E and Fornari M. Plasma Transferred Arc deposition of powdered high performances alloys: process parameters optimisation as a function of alloy and geometrical

configuration. *Surface and Coatings Technology*. 2004; 187(2-3):265-271. http://dx.doi.org/10.1016/j.surfcoat.2004.02.013.

9. Kesavan D and Kamaraj M. Influence of aging treatment on microstructure, wear and corrosion behavior of a nickel base hardfaced coating. *Wear*. 2011; 272(1):7-17. http://dx.doi.org/10.1016/j.wear.2011.05.041.
10. Hou QY, Huang ZY, Shi N and Gao JS. Effects of molybdenum on the microstructure and wear resistance of nickel-based hardfacing alloys investigated using Rietveld method. *Journal of Materials Processing Technology*. 2009; 209(6):2767-2772. http://dx.doi.org/10.1016/j.jmatprotec.2008.06.025.
11. Guoqing C, Xuesong F, Yanhui W, Shan L and Wenlong Z. Microstructure and wear properties of nickel-based surfacing deposited by plasma transferred arc welding. *Surface and Coatings Technology*. 2013; 228(Suppl 1):S276-S282. http://dx.doi.org/10.1016/j.surfcoat.2012.05.125.
12. Gonçalves e Silva, RHG, Dutra, JC. PTA-P process - a literature review as basis for innovations. Part 1 of 2: constructive elements. *Soldagem e Inspeção*. 2012; 17(1):76-85. http://dx.doi.org/10.1590/S0104-92242012000100011.
13. Yaedu AE and D'Oliveira ASCM. Cobalt based alloy PTA hardfacing on different substrate steels. *Materials Science and Technology*. 2005; 21(4):459-466. http://dx.doi.org/10.1179/174328413X13789824293380.
14. Reinaldo PR and D'Oliveira ASCM. NiCrSiB Coatings Deposited by Plasma Transferred Arc on Different Steel Substrates. *Journal of Materials Engineering and Performance*. 2013; 22(2):590-597. http://dx.doi.org/10.1007/s11665-012-0271-7.
15. Antoszczyszyn TJ, Paes RMG, Oliveira ASCM and Scheid A. Impact of Dilution on the Microstructure and Properties of Ni-based 625 Alloy Coatings. *Soldagem e Inspeção*. 2014; 19(2):134-144. http://dx.doi.org/10.1590/0104-9224/SI1902.05.
16. Aziz I. Asphahani. corrosion of nickel-base alloys. In: ASM International. *Corrosion.* Ohio: Materials Park; 1993. p. 641-657.
17. Rabinowicz E. *Friction and wear of materials*. 2nd ed. New York: Wiley Interscience; 1995. p. 143-190.